UMYU Scientifica, Vol. 5 NO. 1, March 2026, Pp 243 – 256
https://doi.org/10.56919/usci.2651.020
ISSN: 2955 – 1145 (print); 2955 – 1153 (online)
A periodical of the Faculty of Natural and Applied Sciences, UMYU, Katsina

ORIGINAL RESEARCH ARTICLE

Analytical Approximation of a Cholera–Typhoid Co-Infection Model with Environmental Reservoirs and Delays Using the Homotopy Perturbation Method

Abdu Sagir Masanawa[1], Chinenye Nworah[2]*, Yusuf. A Bichi[3] and Joel M. Orverem[4]
[1,2,3,4]Department of Mathematics, Federal University Dutsin-Ma, Katsina State, Nigeria

ABSTRACT

Cholera and typhoid fever remain major waterborne diseases in developing regions due to poor sanitation, unsafe water, and weak health systems. We formulated and analyzed a nonlinear deterministic model to study cholera and typhoid co-infection in a uniformly mixing population, incorporating person-to-person and bacteria-mediated transmission, latency, and environmental reservoirs. Existence and uniqueness of solutions were established using Lipschitz conditions, confirming the model's stability. The basic reproduction number, R_0, was derived using the next-generation matrix to determine disease persistence. Explicitly, for cholera and typhoid are given by $R_c = \frac{\mu_{C_2} S_H}{N k_3} + \frac{\varphi_{C_1} S_H}{K_C \delta_C} + \frac{\varrho_C \mu_{C_2} S_H}{N k_5}$ and $R_T = \frac{\mu_{T_2} S_H}{N k_4} + \frac{\varphi_{T_1} S_H}{K_T \delta_T} + \frac{\varrho_T \mu_{T_2} S_H}{N k_5}$ respectively, where S_H is the susceptible population, N the total population, μ infection rates, φ transmission coefficients, K bacterial constants, δ pathogen decay rates, ϱ vaccination effect, and k_i auxiliary constants. Analytical approximate solutions incorporating incubation delays were obtained using the Homotopy Perturbation Method (HPM), and validated against the Adomian Decomposition Method (ADM) and high-precision numerical simulations. Sensitivity analysis via Tornado charts shows vaccination rates, recovery, and environmental transmission parameters are most influential in controlling R_0. Numerical simulations show that vaccination, effective treatment, and reduced environmental contamination significantly lower infection prevalence and bacterial concentrations. Susceptible populations decline initially due to infection, while vaccinated and recovered compartments increase. Co-infected populations remain low under combined interventions, highlighting the importance of integrated public health strategies including vaccination, treatment, and sanitation for controlling cholera–typhoid co-infections in endemic regions. The study demonstrates HPM's effectiveness and provides quantitative insights for controlling cholera–typhoid co-infections.

ARTICLE HISTORY

Received December 13, 2025
Accepted March 09, 2026
Published March 25, 2026

KEYWORDS

Cholera and Typhoid co-infection, Mathematical modelling, Nonlinear differential equations, Reproduction number, Existence and uniqueness, Positivity of solution, Homotopy Perturbation Method (HPM).

INTRODUCTION

Cholera and typhoid fever are persistent waterborne diseases in low- and middle-income countries, fueled by poor sanitation, limited safe water, and weak health systems (Ali et al., 2015). Cholera, caused by *Vibrio cholerae*, leads to severe watery diarrhea and rapid dehydration, while typhoid, caused by *Salmonella Typhi*, results in prolonged fever and gastrointestinal complications (Matsebula & Nyabadza, 2022) Cholera, caused by *Vibrio cholerae*, leads to severe watery diarrhea and rapid dehydration, with an incubation period typically between 0.5–4.4 days (median ~1.4 days) (Azman et al., 2013) , while typhoid, caused by *Salmonella Typhi*, results in prolonged fever and gastrointestinal complications, with an incubation period of 6-30 days (CDC, 2024).

Both spread through the fecal-oral route, often through contaminated water or food, and co-infections are common in endemic regions. In Nigeria, cholera is concentrated in northern and north-eastern areas, especially during rainy seasons when flooding contaminates water sources (Ogunniyi et al., 2025). Typhoid is more widespread, with higher incidence in urban centers due to population density and inadequate waste management (Marks et al., 2017; Stanaway et al., 2019). Limited diagnostic capacity further underestimates typhoid burden, highlighting the need for improved water, sanitation, and surveillance. Furthermore, studies have highlighted increasing antimicrobial resistance in *Vibrio cholerae*, complicating treatment and control (Rabiu et al., 2022), while medicinal plant extracts have shown potential antibacterial activity against diarrheal pathogens, including *V. cholerae* and *Salmonella enterica* serovars (Zamfarawa, et al., 2024).

Correspondence: Chinenye Nworah. Department of Mathematics, Federal University Dutsin-Ma, Katsina State, Nigeria. ✉ nchinenye@fudutsinma.edu.ng.
How to cite: Sagir, A. M., Mworah, C., Bichi, Y. A. & Orverem, J. M. (2026). Analytical Approximation of a Cholera–Typhoid Co-Infection Model with Environmental Reservoirs and Delays Using the Homotopy Perturbation Method. *UMYU Scientifica*, 5(1), 243 – 256. https://doi.org/10.56919/usci.2651.020

Mathematical modeling is essential for understanding infectious disease dynamics, especially co-infections. Semi-analytical methods like the Homotopy Perturbation Method (HPM) are increasingly used to obtain explicit solutions without small-parameter assumptions. (Kolawole & Adebayo, 2025), applied HPM to an age-structured cholera model with vaccination, highlighting demographic impacts on intervention outcomes used HPM on a SIRD cholera model, comparing analytical and Runge-Kutta solutions. (Kumar, P. V. et al., 2024), applied HPM to a malaria-cholera co-infection model to derive approximate solutions and control strategies. (Alshomrani et al., 2024), demonstrated HPM's accuracy in solving nonlinear epidemic systems, and (Popoola et al., 2023), applied it to a fractional-order typhoid model. Methodologically, numerical and mathematical approaches used in other studies, such as modelling Monkeypox transmission with human-rodent interactions, provide guidance for structuring compartmental models and performing sensitivity analysis (Bolaji et al., 2024). Finally, (Matsebula & Nyabadza, 2022), examined cholera and typhoid co-infection dynamics, emphasizing environmental reservoirs and human contact patterns.

Although, (Matsebula & Nyabadza, 2022) modeled cholera–typhoid co-infection, their study did not include exposed or vaccinated compartments, limiting analysis of incubation and immunization effects. This study extends prior work by incorporating vaccinated (V_C, V_T) classes and exposed (E_C, E_T) class, along with delays and environmental reservoirs for both pathogens. This allows examination of vaccination impact, latent periods, and co-infection dynamics, providing new epidemiological insights, such as modified threshold behavior and differential outcomes under intervention scenarios. The use of the homotopy perturbation method (HPM) provides analytical approximations that clarify how key epidemiological and intervention parameters shape disease progression, complementing numerical simulations.

MATERIALS AND METHODS

2.1 Model Diagram

The schematic diagram in Figure 1, presents the cholera-typhoid co-infection structure, showing interactions between human compartments and environmental bacteria. The human population is grouped into susceptible, vaccinated, exposed, infected, co-infected, and recovered classes, with movements between them governed by infection, vaccination, recovery, loss of immunity, and mortality. Bacterial concentrations in the environment increase through shedding from exposed and infectious individuals and decrease through natural decay.

2.2 The Model Formulation

A cholera-typhoid co-infection model was developed by incorporating both human and bacterial populations. The total human population at time t, is subdivided into $S_H, V_C, V_T, E_C, E_T, I_C, I_T, I_{TC}, R_C, R_T$ and R_{TC} . S_H increases through recruitment at a constant rate Λ, as well as loss of immunity from recovered and vaccinated individuals.

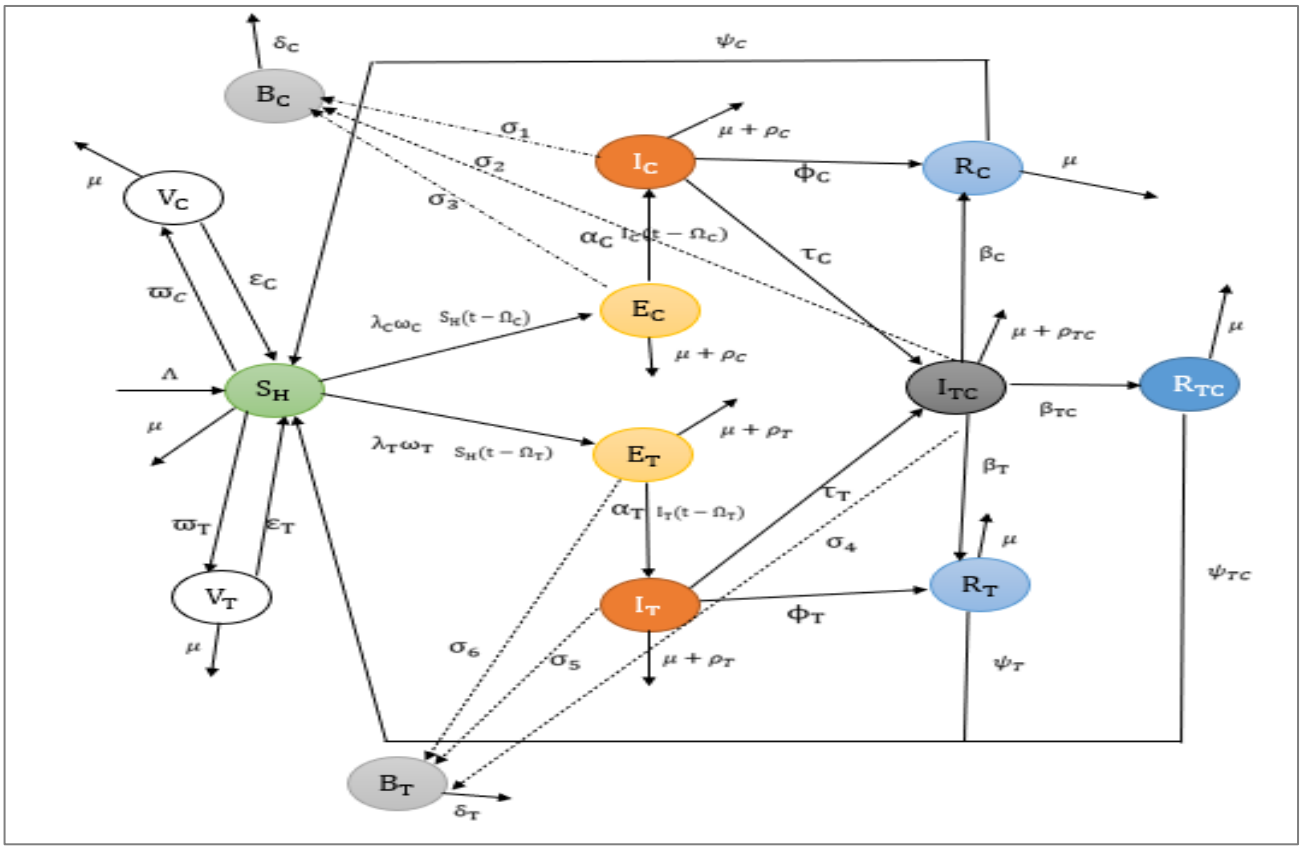

Figure 1. Schematic diagram of the Model.

It decreases due to new infections, vaccination, and natural mortality μ. E_C, E_T are generated through effective contact with infectious individuals. They progress to their respective infectious classes or recover, and are reduced by mortality. I_C, I_T arise from exposed individuals and may either recover, progress to I_{TC}, or die due to disease or natural causes. I_{TC} are generated from secondary infections of I_C or I_T, and may recover or die. V_C, V_T are generated from the S_H through immunization and reduced by waning immunity and mortality. R_C, R_T are generated through treatment of their respective infected classes, after which they may lose immunity and return to the susceptible class or die naturally. Finally, B_C, B_T are produced by shedding from infectious and exposed individuals, and decay naturally over time. These interactions lead to the nonlinear differential equations (1) to (13), representing the cholera-typhoid co-infection dynamics.

$$\frac{dS_H}{dt} = \Lambda - (\lambda_C + \lambda_T + \varpi_T + \varpi_C + \mu)S_H + \psi_C R_C + \psi_{TC} R_{TC} + \psi_T R_T + \varepsilon_C V_C + V_T \varepsilon_T \quad (1)$$

$$\frac{dV_C}{dt} = \varpi_C S_H - (\varepsilon_C + \mu)V_C \quad (2)$$

$$\frac{dV_T}{dt} = \varpi_T S_H - (\varepsilon_T + \mu)V_T \quad (3)$$

$$\frac{dE_C}{dt} = \lambda_C S_H - \mathrm{k}_1 E_C \quad (4)$$

$$\frac{dE_T}{dt} = \lambda_T S_H - \mathrm{k}_2 E_T \quad (5)$$

$$\frac{dI_C}{dt} = \alpha_C E_C - \mathrm{k}_3 I_C(t - \Omega_C) \quad (6)$$

$$\frac{dI_T}{dt} = \alpha_T E_T - \mathrm{k}_4 I_T(t - \Omega_T) \quad (7)$$

$$\frac{dI_{TC}}{dt} = \tau_T I_T + \tau_C I_C - \mathrm{k}_5 I_{TC} \quad (8)$$

$$\frac{dR_C}{dt} = \phi_C I_C - (\mu + \psi_C)R_C \quad (9)$$

$$\frac{\mathrm{d}R_T}{dt} = \phi_T I_T - (\mu + \psi_T)R_T \quad (10)$$

$$\frac{dR_{TC}}{dt} = \phi_{TC} I_{TC} - (\mu + \psi_{TC})R_{TC} \quad (11)$$

$$\frac{dB_C}{dt} = \beta_C B_C \left(1 - \frac{B_C}{K_C}\right) + \sigma_2 I_C + \sigma_3 E_C + \sigma_1 I_{TC} - \delta_C B_C \quad (12)$$

$$\frac{dB_T}{dt} = \beta_T B_T \left(1 - \frac{B_T}{K_T}\right) + \sigma_5 I_T + \sigma_6 E_T + \sigma_4 I_{TC} - \delta_T B_T \quad (13)$$

Where

$\mathrm{k}_1 = \alpha_\mathrm{C} + \mu + \rho_\mathrm{C} + \sigma_3$
$\mathrm{k}_2 = \alpha_\mathrm{T} + \mu + \rho_\mathrm{T} + \sigma_6$
$\mathrm{k}_3 = \phi_\mathrm{C} + \mu + \rho_\mathrm{C} + \tau_\mathrm{C} + \sigma_1$
$\mathrm{k}_4 = \phi_\mathrm{T} + \mu + \rho_\mathrm{T} + \tau_\mathrm{T} + \sigma_5$
$\mathrm{k}_5 = \phi_\mathrm{TC} + \mu + \rho_\mathrm{CT} + \sigma_2 + \sigma_4$.

The forces of infection are written as:

$$\lambda_C = \frac{\varphi_{C_1} B_C}{B_C + K_C} + \frac{\mu_{C_2}(I_C + \varrho_C I_{CT})}{N}, \quad \lambda_T = \frac{\varphi_{T_1} B_T}{B_T + K_T} + \frac{\mu_{T_2}(I_T + \varrho_T I_{CT})}{N}$$

$$\tau_C = \frac{\varphi_{C_3} B_C}{B_C + K_C} + \frac{\mu_{C_4}(I_C + \varrho_C I_{CT})}{N}, \quad \tau_T = \frac{\varphi_{T_3} B_T}{B_T + K_T} + \frac{\mu_{T_4}(I_T + \varrho_T I_{CT})}{N}$$

Table 1. Description of Key Model Variables

Variables	Description
S_H	Susceptible humans
E_C, E_T	Cholera and typhoid exposed humans respectively
V_C, V_T	Cholera, typhoid vaccinated humans respectively
I_T, I_C, I_{TC}	Typhoid infected, cholera infected and coinfected humans respectively
R_C, R_T, R_{TC}	Cholera recovered, Typhoid recovered, Cholera-typhoid recovered
B_C, B_T	Cholerae Typhi concentration and Salmonella bacteria concentration

ANALYSIS OF THE MODEL

3.1 Existence and uniqueness of solution

We establish the existence and uniqueness of solutions to the proposed system of equations (1) to (13) subject to the initial conditions:

$\mathrm{S_H}(0) = \mathrm{V_C}(0) = \mathrm{V_T}(0) = \mathrm{E_C}(0) = \mathrm{E_T}(0) = \mathrm{I_C}(0) = \mathrm{I_T}(0) = \mathrm{I_{TC}}(0) = \mathrm{R_C}(0) = \mathrm{R_T}(0) = \mathrm{R_{TC}}(0) = \mathrm{B_C}(0) = \mathrm{B_T}(0)$ are satisfied.

Theorem 1

The system of differential equations (1) to (13), possesses unique solution in the domain $\Omega = \{(X,t): (X_i < b_0, 0 \leq \mathrm{t} \leq a_0\}$ where $X = \left(\mathrm{S_H}(t), \mathrm{V_C}(t), \mathrm{V_T}(t), \mathrm{E_C}(t), \mathrm{E_T}(t), \mathrm{I_C}(t), \mathrm{I_T}(t), \mathrm{I_{TC}}(t), \mathrm{R_C}(t), \mathrm{R_T}(t), \mathrm{R_{TC}}(t), \mathrm{B_C}(t), \mathrm{B_T}(t)\right)$, and all parameters $\Lambda, \psi_C, \psi_T, \varpi_C, \varpi_T, \tau_\mathrm{C}, \tau_\mathrm{T}$ are strictly positives constants with $a_0 b_0 < \infty$.

Proof

The system can be rewritten in compact vector form

$\frac{dX}{dt}\mathrm{F_i}(X,t),\ X(0) = X_0.$

We then define

$\mathrm{F_i}(\mathrm{S_H}(0), \mathrm{V_C}(0), \mathrm{V_T}(0), \mathrm{E_C}(0), \mathrm{E_T}(0), \mathrm{I_C}(0), \mathrm{I_T}(0), \mathrm{I_{TC}}(0), \mathrm{R_C}(0), \mathrm{R_T}(0), \mathrm{R_{TC}}(0), \mathrm{B_C}(0)\ , \mathrm{B_T}(0))$ as follows:

$$\mathrm{F_1}(t, \mathrm{S_H}(0), \mathrm{V_C}(0), \mathrm{V_T}(0), \mathrm{E_C}(0), \mathrm{E_T}(0), \mathrm{I_C}(0), \mathrm{I_T}(0), \mathrm{I_{TC}}(0), \mathrm{R_C}(0), \mathrm{R_T}(0), \mathrm{R_{TC}}(0), \mathrm{B_C}(0)\ , \mathrm{B_T}(0)) = \Lambda - (\lambda_\mathrm{C} + \lambda_\mathrm{T} + \varpi_T + \varpi_C + \delta)\mathrm{S_H} + \psi_C R_C + \psi_{TC} R_{TC} + \psi_T R_T + \varepsilon_C V_C + V_T \varepsilon_T$$

$$\mathrm{F_2}(t, \mathrm{S_H}(0), \mathrm{V_C}(0), \mathrm{V_T}(0), \mathrm{E_C}(0), \mathrm{E_T}(0), \mathrm{I_C}(0), \mathrm{I_T}(0), \mathrm{I_{TC}}(0), \mathrm{R_C}(0), \mathrm{R_T}(0), \mathrm{R_{TC}}(0), \mathrm{B_C}(0)\ , \mathrm{B_T}(0)) = \varpi_C \mathrm{S_H} - (\varepsilon_\mathrm{C} + \delta)\mathrm{V_C}$$

$$\mathrm{F_3}(t, \mathrm{S_H}(0), \mathrm{V_C}(0), \mathrm{V_T}(0), \mathrm{E_C}(0), \mathrm{E_T}(0), \mathrm{I_C}(0), \mathrm{I_T}(0), \mathrm{I_{TC}}(0), \mathrm{R_C}(0), \mathrm{R_T}(0), \mathrm{R_{TC}}(0), \mathrm{B_C}(0)\ , \mathrm{B_T}(0)) = \varpi_T \mathrm{S_H} - (\varepsilon_T + \delta)V_T$$

$$\mathrm{F_4}(t, \mathrm{S_H}(0), \mathrm{V_C}(0), \mathrm{V_T}(0), \mathrm{E_C}(0), \mathrm{E_T}(0), \mathrm{I_C}(0), \mathrm{I_T}(0), \mathrm{I_{TC}}(0), \mathrm{R_C}(0), \mathrm{R_T}(0), \mathrm{R_{TC}}(0), \mathrm{B_C}(0)\ , \mathrm{B_T}(0)) = \lambda_C \mathrm{S_H} - \mathrm{k_1 E_C}$$

$$\mathrm{F_5}(t, \mathrm{S_H}(0), \mathrm{V_C}(0), \mathrm{V_T}(0), \mathrm{E_C}(0), \mathrm{E_T}(0), \mathrm{I_C}(0), \mathrm{I_T}(0), \mathrm{I_{TC}}(0), \mathrm{R_C}(0), \mathrm{R_T}(0), \mathrm{R_{TC}}(0), \mathrm{B_C}(0)\ , \mathrm{B_T}(0)) = \lambda_T \mathrm{S_H} - \mathrm{k_2 E_T}$$

$$\mathrm{F_6}(t, \mathrm{S_H}(0), \mathrm{V_C}(0), \mathrm{V_T}(0), \mathrm{E_C}(0), \mathrm{E_T}(0), \mathrm{I_C}(0), \mathrm{I_T}(0), \mathrm{I_{TC}}(0), \mathrm{R_C}(0), \mathrm{R_T}(0), \mathrm{R_{TC}}(0), \mathrm{B_C}(0)\ , \mathrm{B_T}(0)) = \alpha_\mathrm{C} \mathrm{E_C} - \mathrm{k_3 I_C}(\mathrm{t} - \Omega_\mathrm{C})$$

$$\mathrm{F_7}(t, \mathrm{S_H}(0), \mathrm{V_C}(0), \mathrm{V_T}(0), \mathrm{E_C}(0), \mathrm{E_T}(0), \mathrm{I_C}(0), \mathrm{I_T}(0), \mathrm{I_{TC}}(0), \mathrm{R_C}(0), \mathrm{R_T}(0), \mathrm{R_{TC}}(0), \mathrm{B_C}(0)\ , \mathrm{B_T}(0)) = \alpha_\mathrm{T} \mathrm{E_T} - \mathrm{k_4 I_T}(\mathrm{t} - \Omega_\mathrm{T})$$

$$\mathrm{F_8}(t, \mathrm{S_H}(0), \mathrm{V_C}(0), \mathrm{V_T}(0), \mathrm{E_C}(0), \mathrm{E_T}(0), \mathrm{I_C}(0), \mathrm{I_T}(0), \mathrm{I_{TC}}(0), \mathrm{R_C}(0), \mathrm{R_T}(0), \mathrm{R_{TC}}(0), \mathrm{B_C}(0)\ , \mathrm{B_T}(0)) = \tau_\mathrm{T} \mathrm{I_T} + \tau_\mathrm{C} \mathrm{I_C} - \mathrm{k_5 I_{TC}}$$

$$\mathrm{F_9}(t, \mathrm{S_H}(0), \mathrm{V_C}(0), \mathrm{V_T}(0), \mathrm{E_C}(0), \mathrm{E_T}(0), \mathrm{I_C}(0), \mathrm{I_T}(0), \mathrm{I_{TC}}(0), \mathrm{R_C}(0), \mathrm{R_T}(0), \mathrm{R_{TC}}(0), \mathrm{B_C}(0)\ , \mathrm{B_T}(0)) = \phi_\mathrm{C} \mathrm{I_C} - (\delta + \psi_C)\mathrm{R_C}$$

$$\mathrm{F_{10}}(t, \mathrm{S_H}(0), \mathrm{V_C}(0), \mathrm{V_T}(0), \mathrm{E_C}(0), \mathrm{E_T}(0), \mathrm{I_C}(0), \mathrm{I_T}(0), \mathrm{I_{TC}}(0), \mathrm{R_C}(0), \mathrm{R_T}(0), \mathrm{R_{TC}}(0), \mathrm{B_C}(0)\ , \mathrm{B_T}(0)) = \phi_\mathrm{T} \mathrm{I_T} - (\delta + \psi_T)\mathrm{R_T}$$

$$\mathrm{F_{11}}(t, \mathrm{S_H}(0), \mathrm{V_C}(0), \mathrm{V_T}(0), \mathrm{E_C}(0), \mathrm{E_T}(0), \mathrm{I_C}(0), \mathrm{I_T}(0), \mathrm{I_{TC}}(0), \mathrm{R_C}(0), \mathrm{R_T}(0), \mathrm{R_{TC}}(0), \mathrm{B_C}(0)\ , \mathrm{B_T}(0)) = \phi_\mathrm{TC} \mathrm{I_{TC}} - (\delta + \psi_{TC})\mathrm{R_{TC}}$$

$$\mathrm{F_{12}}(t, \mathrm{S_H}(0), \mathrm{V_C}(0), \mathrm{V_T}(0), \mathrm{E_C}(0), \mathrm{E_T}(0), \mathrm{I_C}(0), \mathrm{I_T}(0), \mathrm{I_{TC}}(0), \mathrm{R_C}(0), \mathrm{R_T}(0), \mathrm{R_{TC}}(0), \mathrm{B_C}(0)\ , \mathrm{B_T}(0)) = \beta_C B_C \left(1 - \frac{B_C}{K_C}\right) + \sigma_2 \mathrm{I_C} + \sigma_3 \mathrm{E_C} + \sigma_1 \mathrm{I_{TC}} - \delta_\mathrm{C} \mathrm{B_C}$$

$$\mathrm{F_{13}}(t, \mathrm{S_H}(0), \mathrm{V_C}(0), \mathrm{V_T}(0), \mathrm{E_C}(0), \mathrm{E_T}(0), \mathrm{I_C}(0), \mathrm{I_T}(0), \mathrm{I_{TC}}(0), \mathrm{R_C}(0), \mathrm{R_T}(0), \mathrm{R_{TC}}(0), \mathrm{B_C}(0)\ , \mathrm{B_T}(0)) = \beta_T B_T \left(1 - \frac{B_T}{K_T}\right) + \sigma_5 \mathrm{I_T} + \sigma_6 \mathrm{E_T} + \sigma_4 \mathrm{I_{TC}} - \delta_\mathrm{T} \mathrm{B_T}$$

Since X is bounded, then $\mathrm{F_i}(X,t) = j = 1,2,3,\ldots,13$ is defined and continuous for all points $\mathrm{F_i}(X,t) = j = 1,2,3,\ldots,13$ in Ω . since $\mathrm{F_i}(X,t)$ are continuous in Ω they take their maximum in Ω. Let this maximum be defined by

$$\sup_{(t,\underline{\mathrm{U}})\in\Omega} \left|\mathrm{F_i}(t, \underline{\mathrm{U}})\right| = j = 1,2,3,\ldots,13$$

Hence $\mathrm{g_i}\left(\underline{\mathrm{U}}, t\right)$ is describe and continuous if there exist an M', such that $|\mathrm{F_i}(X,t)| \leq M'$ and $\delta = \mathrm{Min}\left(\mathrm{a_0}, \frac{\mathrm{b_0}}{m}\right)$ denote $\mathrm{g_i}\left(\underline{\mathrm{U}}, t\right)$ in the neighborhood of Ω remain bounded and continuous, the solutions of the equations is unique in the interval $|t| < \delta$.

3.2 Positivity of Solution

Since the model describes human and bacterial populations, it is necessary to show that all state variables remain non-negative for all $t \geq 0$, provided the initial conditions are non-negative.

Proof.

Consider the susceptible population equation

$\frac{\mathrm{dS_H}}{\mathrm{dt}} = \Lambda - (\lambda_\mathrm{C} + \lambda_\mathrm{T} + \varpi_T + \varpi_C + \mu)\mathrm{S_H} + \psi_C \mathrm{R_C} + \psi_{TC} \mathrm{R_{TC}} + \psi_T \mathrm{R_T} + \varepsilon_C V_C + V_T \varepsilon_T$

Ignoring the non-negative inflow terms gives

$$\frac{\mathrm{dS_H}}{\mathrm{dt}} \geq -(\lambda_\mathrm{C} + \lambda_\mathrm{T} + \varpi_T + \varpi_C + \mu)\mathrm{S_H}$$

Solving yields

$S_H(t) \geq S_H(0)e^{(-\int(\lambda_C+\lambda_T+\varpi_T+\varpi_C+\mu)ds)} \geq 0$, for all $t \geq 0$.

Using the same comparison argument, the vaccinated classes V_C, V_T, exposed classes E_C, E_C, infected classes I_C, I_T, I_{TC}, and recovered classes R_C, R_{TC} satisfy inequalities of the form

$$\frac{dx}{dt} \geq -kx$$

Where $k > 0$, implying $x \geq x(0)e^{-kt} \geq 0, \forall\, t \geq 0$.

For the bacterial populations B_C and B_T, the logistic growth with non-negative shedding terms ensures that

$$B_C(t) \geq 0, B_T(t) \geq 0 \qquad \forall\, t \geq 0,$$

Whenever $B_C(0), B_T(0) \geq 0$

Hence, all state variables of the cholera–typhoid co-infection model remain non-negative for all $t \geq 0$.

3.3 Reproduction number R_0

The basic reproduction number R_0 is defined here in the average number of people that cholera, typhoid will initiate in a population of completely infected population. Using

$R_0 < 1 \Longrightarrow$ Cholera and Typhoid Co-infection will die.

$R_0 > 1 \Longrightarrow$ Cholera and Typhoid Co-infection will persist within a community.

We apply the (van den Driessche & Watmough, 2002) method to equations (4)–(8), (12)–(13), which govern infection dynamics.

At the disease-free equilibrium:

$S_H^* = \frac{\Lambda}{\mu}, E_C = E_T = I_C = I_T = I_{TC} = B_C = B_T = 0$

All vaccinated and recovered classes may be nonzero but do not affect new infections.

Linearising the forces of infection near disease free equilibrium we have

$\lambda_C = \frac{\varphi_{C_1}}{K_C}B_C + \frac{\mu_{C_2}}{S_H^*}(I_C + \varrho_C I_{CT})$, $\lambda_T = \frac{\varphi_{T_1}}{K_T}B_T + \frac{\mu_{T_2}}{S_H^*}(I_T + \varrho_T I_{CT})$

For each infected compartment x_i:

$$\frac{dx_i}{dt} = F_i(X_I) - V_i(X_I)$$

Where F_i are new infection terms only and V_i are transfers, progression, recovery and death.

Only new infections appear in exposed compartments; all other infected compartments receive no new infections.

Substitute linearized λ_C, λ_T and evaluate at the DFE $(S_H = S_H^*)$:

$$F_{E_C} = \mu_{C_2}(I_C + \varrho_C I_{CT}) + \frac{\varphi_{C_1 S_H^*}}{K_C}B_C$$

$$F_{E_T} = \varphi_{T_2}(I_T + \varrho_T I_{CT}) + \frac{\varphi_{T_1 S_H^*}}{K_T}B_T$$

Ordering the infected variables as $E_C, E_T, I_C, I_T, I_{TC}, B_C, B_T$ we have the matrix for of F, V and V^{-1} :

$$F = \begin{pmatrix} 0 & 0 & \frac{\mu_{C_2}S_H^*}{N} & 0 & \frac{\varrho_C\mu_{C_2}S_H^*}{N} & \frac{\varphi_{C_1}s_H^*}{K_C} & 0 \\ 0 & 0 & 0 & \frac{\mu_{T_2}S_H^*}{N} & \frac{\varrho_T\mu_{T_2}S_H^*}{N} & 0 & \frac{\varphi_{T_1}s_H^*}{K_T} \\ 0 & 0 & 0 & 0 & 0 & 0 & 0 \\ 0 & 0 & 0 & 0 & 0 & 0 & 0 \\ 0 & 0 & \tau_C & \tau_T & 0 & 0 & 0 \\ 0 & 0 & 0 & 0 & 0 & 0 & 0 \\ 0 & 0 & 0 & 0 & 0 & 0 & 0 \end{pmatrix} \tag{14}$$

$$V = \begin{pmatrix} k_1 & 0 & 0 & 0 & 0 & 0 & 0 \\ 0 & k_2 & 0 & 0 & 0 & 0 & 0 \\ -\alpha_c & 0 & k_3 & 0 & 0 & 0 & 0 \\ 0 & -\alpha_T & 0 & k_4 & 0 & 0 & 0 \\ 0 & 0 & 0 & 0 & k_5 & 0 & 0 \\ -\sigma_3 & 0 & -\sigma_2 & 0 & -\sigma_1 & \delta_c & 0 \\ 0 & -\sigma_6 & 0 & -\sigma_5 & -\sigma_4 & 0 & \delta_T \end{pmatrix} \tag{15}$$

$$V^{-1} = \begin{pmatrix} \frac{1}{k_1} & 0 & 0 & 0 & 0 & 0 & 0 \\ 0 & \frac{1}{k_2} & 0 & 0 & 0 & 0 & 0 \\ \frac{\alpha_c}{k_3 k_1} & 0 & \frac{1}{k_3} & 0 & 0 & 0 & 0 \\ 0 & \frac{\alpha_T}{k_2 k_4} & 0 & \frac{1}{k_4} & 0 & 0 & 0 \\ 0 & 0 & 0 & 0 & \frac{1}{k_5} & 0 & 0 \\ \frac{\sigma_2\alpha_c+\sigma_3 k_3}{k_1 k_3 \delta_c} & 0 & \frac{\sigma_2}{k_3\delta_C} & 0 & \frac{\sigma_1}{k_5\delta_C} & \frac{1}{\delta_C} & 0 \\ 0 & \frac{\sigma_5\alpha_T+\sigma_6 k_4}{k_4 k_2 \delta_T} & 0 & \frac{\sigma_5}{k_4\delta_T} & \frac{\sigma_4}{k_5\delta_T} & 0 & \frac{1}{\delta_T} \end{pmatrix} \tag{16}$$

Then the general matrix

$$R_0 = FV^{-1} = \begin{pmatrix} 0 & 0 & \frac{\mu_{C_2} S_H^*}{N k_3} & 0 & \frac{\varrho_C \mu_{C_2} S_H^*}{N k_5} & \frac{\varphi_{C_1} s_H^*}{K_C \delta_C} & 0 \\ 0 & 0 & 0 & \frac{\mu_{T_2} S_H^*}{N k_4} & \frac{\varrho_T \mu_{T_2} S_H^*}{N k_5} & 0 & \frac{\varphi_{T_1} s_H^*}{K_T \delta_T} \\ 0 & 0 & 0 & 0 & 0 & 0 & 0 \\ 0 & 0 & 0 & 0 & 0 & 0 & 0 \\ 0 & 0 & \frac{\tau_C}{k_3} & \frac{\tau_T}{k_4} & 0 & 0 & 0 \\ 0 & 0 & 0 & 0 & 0 & 0 & 0 \\ 0 & 0 & 0 & 0 & 0 & 0 & 0 \end{pmatrix} \tag{17}$$

The eigenvalues which represent the two reproduction numbers, where R_c is the expected number of cholera infection produced by one infectious individual and R_T is the expected number of typhoid infections produced by one infectious individual is written as

$$R_c = \frac{\mu_{C_2} S_H}{N k_3} + \frac{\varphi_{C_1} s_H}{K_C \delta_C} + \frac{\varrho_C \mu_{C_2} S_H}{N k_5} \;,\; R_T = \frac{\mu_{T_2} S_H}{N k_4} + \frac{\varphi_{T_1} s_H}{K_T \delta_T} + \frac{\varrho_T \mu_{T_2} S_H}{N k_5} \tag{18}$$

So that

$$R_0 = \max\{R_C, R_T\}. \tag{19}$$

3.4 Analytical and Numerical Solution of the Delayed Cholera–Typhoid Model

We analyze the cholera–typhoid co-infection model given by equations (1) to (13), which includes discrete time delays Ω_C and Ω_T representing latent infection periods for cholera and typhoid, respectively. The inclusion of delays leads to a system of delay differential equations, a framework commonly used to model incubation effects in infectious disease dynamics (Guglielmi et al., 2022; Raza et al., 2024).

For delay differential equations, it is necessary to prescribe initial history functions for all delayed state variables to ensure existence and uniqueness of solutions.

Let $\Omega_{\max} = \max\{\Omega_C, \Omega_T\}$ for $t \in [-\Omega_{\max}]$, the delayed compartments are prescribed by constant history functions:

$$I_C(t) = I_{C_0}(t) \text{ for } t \in [-\Omega_C, 0], \; I_T(t) = I_{T_0}(t) \text{ for } t \in [-\Omega_T, 0]$$

All other compartments are initialized at $t = 0$ by their respective values:

$$S_H(t) = S_{H_0}(t),\, V_C(t) = V_{C_0}(t), V_T(t) = V_{T_0}(t), E_C(t) = E_{C_0}(t), E_T(t) = E_{T_0}(t), I_{TC}(t) = I_{TC_0}(t), R_C(t) = R_0(t), R_T(t) = R_{T_0}(t), R_{TC}(t) = R_{TC_0}(t), B_C(t) = B_{C_0}(t), B_T(t) = B_{T_0}(t)$$

Constant history functions are routinely used in epidemic models with delays when dynamics before $t = 0$ are assumed to be stable (Raza et al., 2024).

3.5 Application of Homotopy Perturbation Method for Solving the Model Equations

Consider the system of differential equations (1) to (13), with the following initial conditions:

$$S_H(0) = S_{H_0}, V_C(0) = V_{C_0}, V_T(0) = V_{T_0}, E_C(0) = E_{C_0}, E_T(0) = E_{T_0}, I_C(0) = I_{C_0}, I_T(0) = I_{T0}, I_{TC}(0) = I_{T_0}, R_C(0) = R_{C_0}, R_T(0) = R_{T_0}, B_C(0) = B_{C_0}, B_T(0) = B_{T_0}$$

The unknown functions are assumed to admit power series solutions in the embedding parameter p:

$S_H(t,p) = S_{H_0}(t) + PS_{H_1}(t) + P^2S_{H_2}(t) \ldots, V_C(t,p) = V_{C_0}(t) + PV_{C_1}(t) + P^2V_{C_2}(t) \ldots,$ $V_T(t,p) = V_{T_0}(t) + PV_{T_1}(t) + P^2V_{T_2}(t) \ldots, E_C(t,p) = E_{C_0}(t) + PE_{C_1}(t) + P^2E_{C_2}(t) \ldots,$ $E_T(t,p) = E_{T_0}(t) + PE_{T_1}(t) + P^2E_{T_2}(t) \ldots, I_C(t,p) = I_{C_0}(t) + PI_{C_1}(t) + P^2I_{C_2}(t) \ldots,$ $I_T(t,p) = I_{T_0}(t) + PI_{T_1}(t) + P^2I_{T_2}(t) \ldots, I_{TC}(t,p) = I_{TC_0}(t) + PI_{TC_1}(t) + P^2I_{TC_2}(t) \ldots,$ $R_C(t,p) = R_{C_0}(t) + PR_{C_1}(t) + P^2R_{C_2}(t) \ldots, R_T(t,p) = R_{T_0}(t) + PR_{T_1}(t) + P^2R_{T_2}(t) \ldots,$ $R_{TC}(t,p) = R_{TC_0}(t) + PR_{TC_1}(t) + P^2R_{TC_2}(t) \ldots, B_C(t,p) = B_{C_0}(t) + PB_{C_1}(t) + P^2B_{C_2}(t) \ldots,$ $B_T(t,p) = B_{T_0}(t) + PB_{T_1}(t) + P^2B_{T_2}(t) \ldots$

For equation (1) which is the susceptible human compartment, the governing equation is written as

$\frac{dS_H}{dt} - F_{S_H}(t,p) + G_{S_H}S_H = 0$

where

$FS_H(t,p) = \Lambda + \psi_C R_C(t,p) + \psi_{TC} R_{TC}(t,p) + \psi_T R_T(t,p) + \varepsilon_C V_C(t,p) + \varepsilon_T V_T(t,p)$ and

$GS_H = \lambda_C \omega_C + \lambda_T \omega_T + \varpi_T + \varpi_C + \mu.$

The Homotopy equation is then constructed as

$(1-p)\frac{d\mathrm{Y}}{dt} + p\left(\frac{d\mathrm{Y}}{dt} - F_{S_H}(t,p) + G_{S_H}\mathrm{Y}\right) = 0$ which reduces to $\frac{d\mathrm{Y}}{dt} - pF_{S_H}(t,p) + pG_{S_H}\mathrm{Y} = 0$

Assuming a perturbation expansion $S_H(t,p) = S_{H_0}(t) + pS_{H_1}(t) + p^2S_{H_0}(t) + \cdots$, and substituting into the homotopy equation, we collect terms of like powers of p. this yields the recursive relations:

$P^0: \frac{dS_0(t)}{dt} = 0, S_{H,0}(0) = S_{H_0}$

$P^1: \frac{dS_{H_1}(t)}{dt} = FS_{H,0}(t) -, S_H S_{H,0}(t),$

$P^2: \frac{dS_{H_2}(t)}{dt} = FS_{H,1}(t) - GS_H S_{H,1}(t),\ S_{H,2}(0) = 0$

$P^k: \frac{dS_{H_k}(t)}{dt} = FS_{H,k-1}(t) - GS_H S_{H,k-1}(t),\ k > 2$

Here $FS_{H,k}(t)$ are the forcing terms expressed as polynomial functions of t.

Hence, we have the Zeroth, first and second order solutions respectively as follows:

$S_{H_0}(t) = S_{H_0},\ \frac{dS_{H_1}(t)}{dt} = K_1,\ \frac{dS_{H_2}(t)}{dt} = (A_F t^2 + B_F t)\ - G_{S_H}K_1 t$ (20)

Integrating, truncating at the second-order term, and assigning $p = 1$ produces the approximate solution.

$S_{H_2}(t) \approx S_{H_0} + K_1 t + \frac{(B_F - G_{S_H}K_1)}{2}t^2 + \frac{A_F}{3}t^3$ (21)

Where

$K_1 = \Lambda + \psi_C R_{C_0} + \psi_{TC} R_{TC_0} + \psi_T R_{T_0} + \varepsilon_C V_{C_0} + \varepsilon_T V_{T_0} - G_{S_H}S_{H_0}$

$A_F = \psi_C A_{R_{C_1}} + \psi_{TC} A_{R_{TC_1}} + \varepsilon_C A_{V_{C_1}} + \varepsilon_T A_{V_{T_1}}$

$B_F = \psi_C B_{R_{C_1}} + \psi_{TC} B_{R_{TC_1}} + \varepsilon_C B_{V_{C_1}} + \varepsilon_T B_{V_{T_1}}$

Applying the same procedure to the equations (2) to (13) yields the following second order approximate solutions:

$V_{C_2}(t) \approx V_{C_0} + K_2 t + \frac{(B_C - G_{V_C}K_2)}{2}t^2 + \frac{A_C}{3}t^3$ (22)

$V_{T_2}(t) \approx V_{T_0} + K_3 t + \frac{(B_T - G_{V_T}K_3)}{2}t^2 + \frac{A_T}{3}t^3$ (23)

$E_{C_2}(t) \approx E_{C_0} + K_4 t + \frac{(B_E - G_{E_C}K_4)}{2}t^2 + \frac{A_E}{3}t^3$ (24)

$E_{T_2}(t) \approx E_{T_0} + K_5 t + \frac{(B_E - G_{E_T}K_5)}{2}t^2 + \frac{A_E}{3}t^3$ (25)

$$I_{C_2}(t) \approx I_{C_0} + K_6 t + \frac{\left(B_I - G_{I_C} K_6\right)}{2} t^2 + \frac{A_I}{3} t^3 \quad (26)$$

$$I_{T_2}(t) \approx I_{T_0} + K_7 t + \frac{\left(B_I - G_{I_T} K_7\right)}{2} t^2 + \frac{A_I}{3} t^3 \quad (27)$$

$$I_{TC_2}(t) \approx I_{TC_0} + K_8 t + \frac{\left(B_I - G_{I_{TC}} K_8\right)}{2} t^2 + \frac{A_I}{3} t^3 \quad (28)$$

$$R_{C_2}(t) \approx R_{C_0} + K_9 t + \frac{\left(B_R - G_{R_C} K_9\right)}{2} t^2 + \frac{A_R}{3} t^3 \quad (29)$$

$$R_{T_2}(t) \approx R_{T_0} + K_{10} t + \frac{\left(B_R - G_{R_T} K_{10}\right)}{2} t^2 + \frac{A_R}{3} t^3 \quad (30)$$

$$R_{TC_2}(t) \approx R_{TC_0} + K_{11} t + \frac{\left(B_R - G_{R_{TC}} K_{11}\right)}{2} t^2 + \frac{A_R}{3} t^3 \quad (31)$$

$$B_{C_2}(t) \approx B_{C_0} + K_{12} t + \frac{\left(B_B - G_{B_C} K_{12}\right)}{2} t^2 + \frac{A_B}{3} t^3 \quad (32)$$

$$B_{T_2}(t) \approx B_{T_0} + K_{13} t + \frac{\left(B_B - G_{B_T} K_{13}\right)}{2} t^2 + \frac{A_B}{3} t^3 \quad (33)$$

3.6 Truncation of the HPM series

The infinite perturbation series must be truncated for analytical tractability. We truncate all series after the second-order term, yielding

$$X(t) \approx X_0(t) + X_1(t) + X_2(t).$$

Second-order truncation has been shown in recent studies to provide accurate approximations with minimal computational effort for compartmental disease models (Rafiullah et al., 2024). The second-order solutions derived in equations (21)–(33) are therefore used throughout the analysis.

3.7 Convergence and error analysis

The convergence of the HPM solutions was examined using the successive-term ratio

$$\rho k(t) = \frac{\|\boldsymbol{X_{k+1}(t)}\|}{\|\boldsymbol{X_k(t)}\|},$$

where $X_k(t)$ denotes the kth order approximation of any state variable. For all compartments and over the entire simulation interval, $\rho k(t) < 1$, indicating rapid convergence of the perturbation series.

To quantify the accuracy of the truncated HPM solutions, comparisons were made with high-precision numerical solutions obtained using an adaptive delay differential equation solver. The discrepancy was measured using the relative L^2error norm

$$\text{Error}(t) = \frac{\|\boldsymbol{X_{HPM}(t) - X_{num}(t)}\|_2}{\|\boldsymbol{X_{num}(t)}\|_2}.$$

where

$X_{HPM}(t)$ is the solution vector using the Homotopy Perturbation Method (HPM) at time t and $X_{num}(t)$ is the numerical solution vector at time t.

3.8 Comparison with Adomian Decomposition Method (ADM)

To verify the accuracy of the Homotopy Perturbation Method (HPM) solutions, we also applied the Adomian Decomposition Method (ADM), following recent practice in epidemic modeling. (Alsubaie et al., 2024). In this approach, the nonlinear terms in each equation are expanded into an infinite series of Adomian polynomials A_n, such that:

$$N(X) = \sum_{n=0}^{\infty} A_n$$

With the successive terms determined recursively by

$$X_{n+1}(t) = \int_0^t [F_X(X_n) - G_X(X_n)]\, dt.$$

The approximate solutions obtained using HPM, ADM, and the numerical solutions will be demonstrated explicitly in the numerical simulation section. This comparison provides an objective basis for assessing the consistency and accuracy of the analytical approximations.

RESULTS AND DISCUSSION

4.1 Numerical Simulation

Numerical simulations were performed to examine the time-dependent behavior of the cholera–typhoid co-infection model, using parameter values derived from Table 3 and epidemiological data obtained from (NCDC and WHO). The resulting trajectories capture the evolution of susceptible, vaccinated, exposed, infected, and recovered classes, as well as the environmental bacterial concentrations. Table 2 shows Model Parameters with Justification.

Table 2. Model Parameters with Justification.

Notation	Description	Value	Reference
Λ	Recruitment rate (Introduction of new susceptible individuals)	100 persons day^{-1}	(Tien & Earn, 2010)
μ	Natural death rate	0.01 day^{-1}	(Yang, 2020)
δ_C, δ_T	Natural death rate of Cholera and typhoid respectively	0.01 day^{-1}	(Kailan Suhuyini & Seidu, 2023; Yang, 2020)
$\phi_C, \phi_T, \phi_{TC}$	Recovery rate from cholera, typhoid and co-infection respectively	0.05 day^{-1}	(Panja, 2019; Wang & Liao, 2012; Yang, 2020)
$\varepsilon_C, \varepsilon_T$	Cholera, typhoid vaccination rate	0.01 day^{-1}	(Kailan Suhuyini & Seidu, 2023; Panja, 2019)
ϖ_C, ϖ_T	Immune lost rate of cholera and typhoid	0.05 day^{-1}	(Kailan Suhuyini & Seidu, 2023; Yang, 2020)
ψ_C, ψ_T	Immunity loss rate of cholera recovered, typhoid recovered	0.02 day^{-1}	(Panja, 2019; Yang, 2020)
ψ_{TC}	Immunity loss rate of cholera and typhoid recovered	0.01 day^{-1}	(Panja, 2019)
K_C, K_T	Concentration of Salmonella bacteria, vibrio cholera in the environment	10,000 cells/ml	(Kailan Suhuyini & Seidu, 2023; Yang, 2020)
ρ_T, ρ_C	Typhoid, cholera	0.01 day^{-1}	(Wang & Liao, 2012; Yang, 2020)
ρ_{CT}	Cholera and typhoid death rate	0.01 day^{-1}	(Panja, 2019)
α_C, α_T	Screening rate of cholera, typhoid infective	0.1 day^{-1}	(Kailan Suhuyini & Seidu, 2023; Yang, 2020)
Ω_T, Ω_C	Delay parameter for typhoid, cholera latent period	3, 6 days	(Azman et al., 2013; CDC, 2024)
$\sigma_1, \sigma_5, \sigma_4, \sigma_2$	Discharge rate of cholera typhoid, cholera-typhoid infectives	0.01 day^{-1}	(Kailan Suhuyini & Seidu, 2023; Panja, 2019)
σ_3, σ_6	Discharge rate of cholera, typhoid exposed	0.01 day^{-1}	(Kailan Suhuyini & Seidu, 2023; Panja, 2019)
ϱ_C, ϱ_T	Cholera, typhoid modification parameter (influencing transmission or progression)	0.62 day^{-1}	(Panja, 2019; Wang & Liao, 2012)
μ_{C_2}, μ_{T_2}	Human-to-human transmission coefficient (cholera and typhoid)	0.3 day^{-1}	(Kailan Suhuyini & Seidu, 2023; Yang, 2020)
$\varphi_{C_1}, \varphi_{T_1}$	Environmental contribution to cholera and typhoid infection	0.5 day^{-1}	(Kailan Suhuyini & Seidu, 2023; Yang, 2020)
β_C, β_T	Growth rate of cholera and typhoid bacteria	0.1 day^{-1}	(Kailan Suhuyini & Seidu, 2023; Yang, 2020)

Table 3. Initial conditions for the cholera–typhoid co-infection simulations.

Compartment	Description	Initial Value
$S_H(0)$	Susceptible humans	10,000
$V_C(0), V_T(0)$	Vaccinated against cholera and typhoid	0
$E_C(0), E_T(0)$	Exposed to cholera and typhoid	100
$I_C(0), I_T(0)$	Infected with cholera, typhoid	50
$I_{TC}(0)$	Coinfected (cholera and typhoid)	0
$R_C(0), R_T(0)$	Recovered from cholera, typhoid	0
$B_C(0), B_T(0)$	Environmental cholera, typhoid bacteria	1×10^3

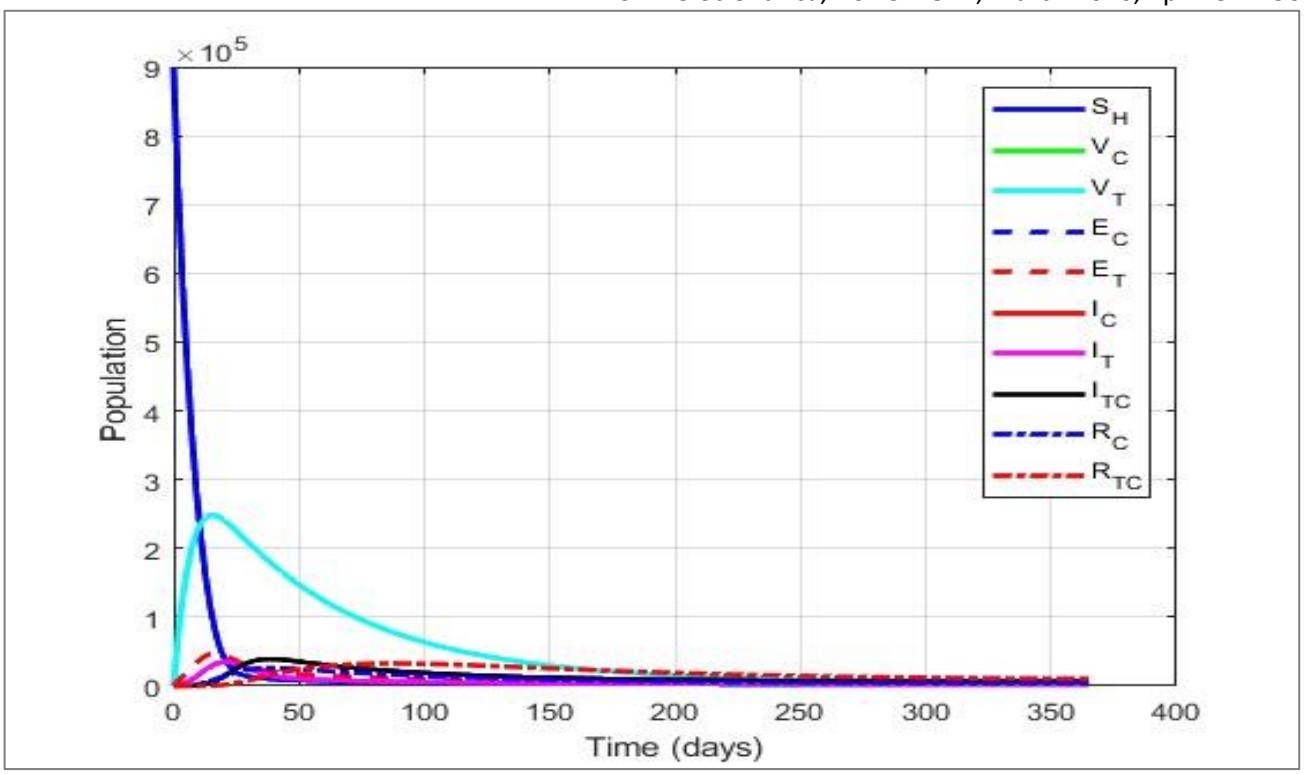

Figure 2. Time-dependent dynamics of the cholera–typhoid co-infection model, illustrating the behavior of susceptible, vaccinated, infected, co-infected, recovered populations under different conditions.

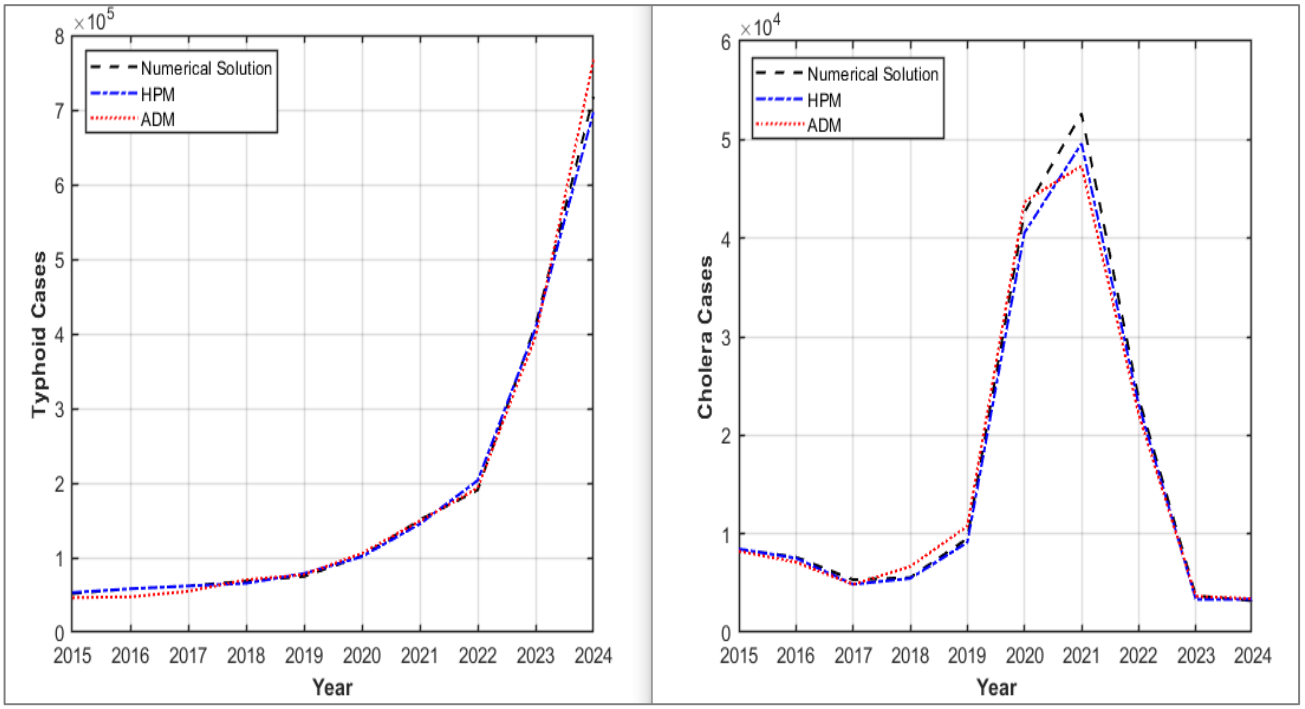

Figure 3. Cholera and typhoid cases predicted by the model using Homotopy Perturbation Method (HPM) and Adomian Decomposition Method (ADM) compared with the high-accuracy numerical Solution

Discussion of Results

The time-dependent dynamics of the cholera–typhoid co-infection model incorporating exposed compartments, vaccination, environmental reservoirs, and time delays are illustrated in Figure 2. The figure presents the temporal evolution of the susceptible, vaccinated, exposed, infected, co-infected, recovered populations, and bacterial concentrations over a one-year simulation period.

As shown in Figure 2, the susceptible population declines rapidly during the early phase of the outbreak due to simultaneous exposure to cholera and typhoid through both human-to-human and environment-to-human transmission pathways. This initial decline is moderated over time by recovery, vaccination, and loss-of-immunity feedback, leading to a gradual stabilization of the susceptible class.

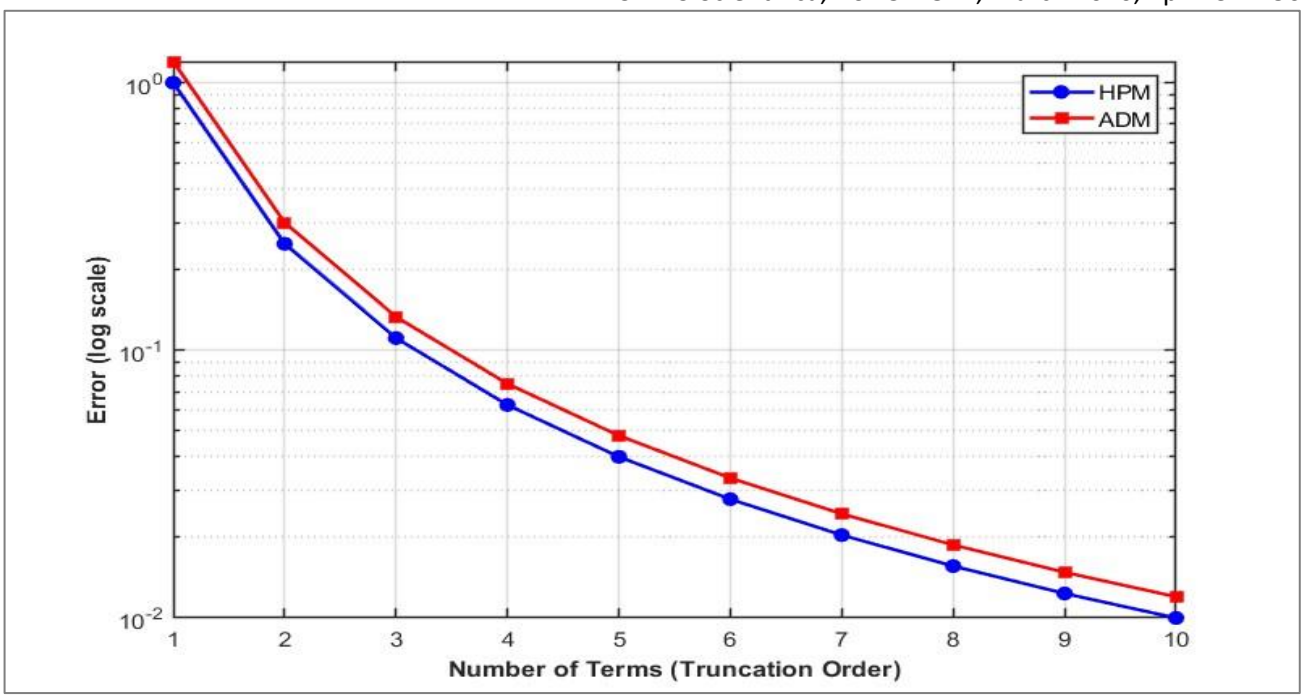

Figure 4. Convergence of HPM and ADM approximations for the cholera–typhoid co-infection model. The plot shows the logarithmic error against truncation term count, indicating rapid convergence of both methods, with HPM achieving slightly faster reduction in error against truncation term count, indicating rapid convergence of both methods, with HPM achieving slightly faster reduction in error compared to ADM

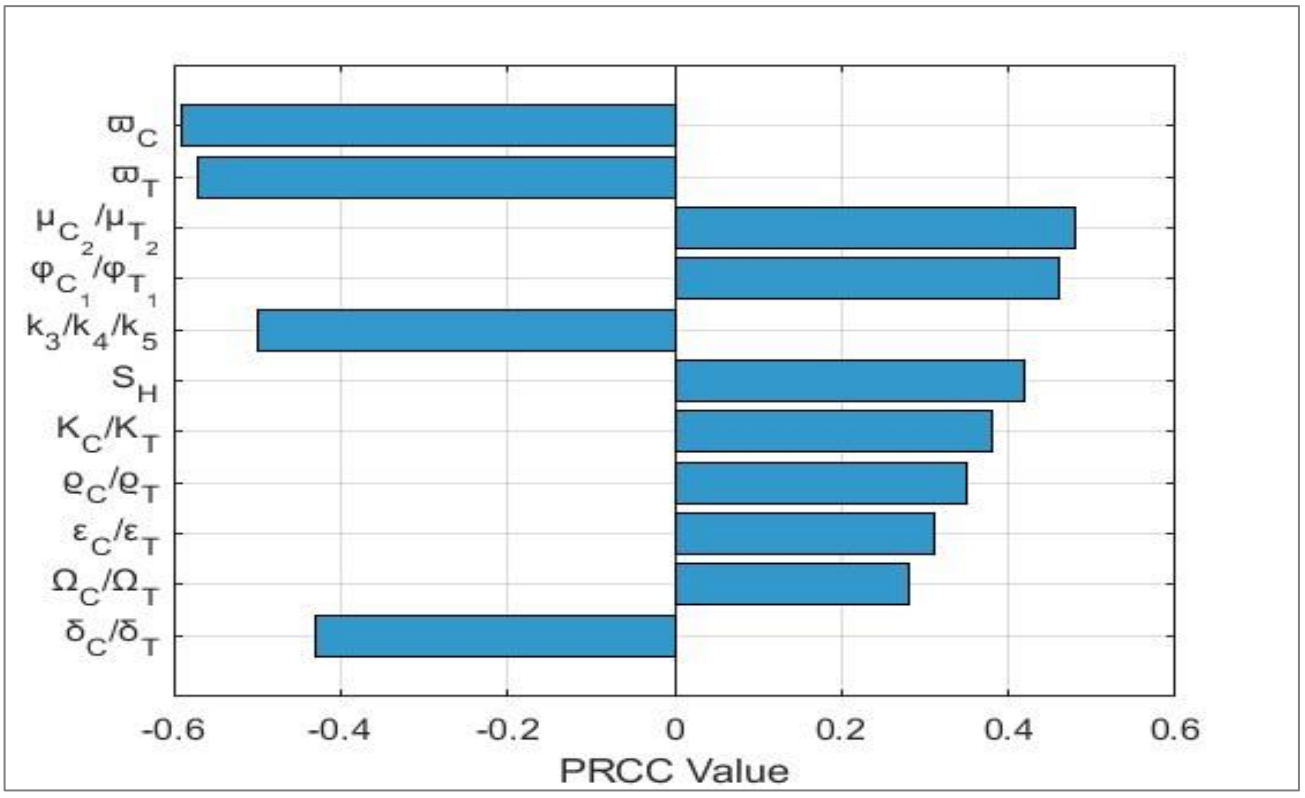

Figure 5. Shows the Tornado chart of R_0 sensitivity, highlighting that cholera and typhoid vaccination rates, human-to-human and environmental transmission, and recovery rates are the most influential parameters controlling epidemic potential.

The vaccinated compartments for cholera and typhoid increase initially and then level off, indicating the long-term impact of vaccination in reducing the pool of susceptible individuals. The exposed classes for cholera and typhoid exhibit a transient rise prior to the onset of symptomatic infection, reflecting the biologically realistic latency period captured by the exposed compartments. This behaviour confirms the importance of including exposed classes, as they introduce a delay between infection acquisition and infectiousness, which is absent in simpler compartmental models.

The infected populations displayed in Figure 2 show a delayed peak relative to the exposed classes, a direct consequence of the incorporated time delays in the infected compartments. The cholera-only and typhoid-only infected classes initially increase due to progression from exposure but subsequently decline as treatment, recovery, and natural mortality dominate. The co-infected compartment reaches its peak later than the single-infection classes, highlighting the cumulative effect of sequential infection pathways and the enhanced disease burden associated with co-infection.

Recovered compartments increase steadily as infections resolve, demonstrating the role of treatment and immune response in disease control. The environmental bacterial concentrations for cholera and typhoid initially rise due to shedding from infected and co-infected individuals but decline over time as bacterial decay and reduced human shedding take effect. This behaviour, also visible in Figure 2, underscores the importance of environmental sanitation in suppressing long-term transmission.

To ensure numerical accuracy and methodological reliability, the semi-analytical solutions obtained using the Homotopy Perturbation Method (HPM) and the Adomian Decomposition Method (ADM) were validated through a convergence analysis, presented in Figure 3. The convergence plot demonstrates a consistent reduction in approximation error as the truncation order increases for both methods, confirming their stability and reliability for the proposed nonlinear delay model.

As observed in Figure 4, HPM consistently yields lower approximation errors than ADM for the same truncation order, indicating faster convergence and higher numerical accuracy. This implies that HPM achieves reliable approximations with fewer series terms, making it computationally efficient for analyzing complex co-infection systems involving delays, multiple compartments, and environmental reservoirs. Overlay plots comparing HPM, ADM, and numerical solutions confirm that both analytical methods reliably reproduce epidemic trends. Integrating these results with the parameter and initial condition tables (Tables 2 and 3) demonstrates both quantitative fidelity to benchmark solutions and analytical transparency.

The sensitivity analysis of R_0 visualised in Figure 5, complements the time-series results by quantitatively identifying the most influential parameters. Vaccination rates for cholera ϖ_C and typhoid ϖ_T show the largest negative correlations with R_0, indicating that increasing vaccination coverage effectively reduces the epidemic potential. Human-to-human and environmental transmission parameters $(\mu_{C_2}, \mu_{T_2}, \varphi_{C_1}, \varphi_{T_1})$ are strongly positively correlated with R_0, highlighting their central role in sustaining transmission. Recovery and removal rates (k_3, k_4, k_5) strongly reduce R_0, whereas co-infection modification factors (ϱ_C, ϱ_T), vaccine waning $(\varepsilon_C, \varepsilon_T)$, and incubation delays (Ω_C, Ω_T) moderately increase R_0. The Tornado chart (Figure 5) clearly ranks these parameters by absolute sensitivity, providing a visual guide for prioritizing interventions.

Taken together, the temporal dynamics, convergence analysis, and sensitivity results validate the proposed model as a robust framework for exploring cholera–typhoid co-infection dynamics. The model captures realistic epidemic patterns through exposed compartments and time delays, quantifies intervention impacts through vaccination and environmental control, and identifies key parameters influencing epidemic thresholds. These insights offer clear policy guidance, emphasizing vaccination programs, rapid treatment, and environmental sanitation as critical strategies to reduce R_0 below unity and prevent sustained outbreaks.

CONCLUSION

A deterministic model for cholera–typhoid co-infection, incorporating exposed compartments, vaccination, environmental reservoirs, and incubation delays, was developed and analyzed. Simulations and analytical approximations (HPM and ADM) show that effective vaccination and reduction of environmental contamination can reduce the basic reproduction number R_0 below 1, preventing sustained outbreaks. Under baseline parameter assumptions, sufficiently high vaccination coverage and substantial reduction in environmental bacterial burden are capable of reducing the basic reproduction number below unity, providing actionable thresholds for public health interventions.

Co-infections persist even after single infections decline, emphasizing the need for timely treatment and rapid response. Delays in incubation produce lagged epidemic peaks, highlighting the importance of early interventions. HPM and ADM reliably reproduce epidemic trends, with HPM demonstrating faster convergence, although differences are quantitatively small (relative L^2 error $< 1\%$).

Sensitivity analysis using Tornado chart demonstrates that vaccination rates, recovery rates, and environmental transmission parameters are the most influential factors controlling R_0. Co-infection factors, vaccine waning, and incubation delays moderately increase R_0, while larger susceptible populations and bacterial carrying capacities further amplify outbreak risk. The Tornado chart visually ranks these parameters, providing clear guidance for prioritizing interventions.

The model assumes uniform mixing, deterministic dynamics, and relies on parameter estimates from literature rather than empirical fitting, limiting generalizability. Delay effects are simplified, and stochastic variability in transmission is not captured.

Extending the model to include stochasticity, optimal control strategies, spatial heterogeneity, and parameter identifiability will improve predictive accuracy and guide more effective intervention policies. Integrated approaches combining vaccination, environmental

sanitation, and rapid clinical response remain essential for controlling cholera–typhoid co-infections and ensuring $R_0 < 1$.

DECLARATIONS

Data Availability

All data, parameters, and materials used in this study are contained within the manuscript. No external datasets were generated or analysed.

Ethics Approval and Consent to Participate

Not applicable. This study is based solely on mathematical modelling and uses no human participants, personal data, animal subjects, or experimental procedures requiring ethical approval.

Consent for Publication

Not applicable. The manuscript does not include any individual person's data.

Competing Interests

The authors declare that they have no competing interests related to this work.

ACKNOWLEDGMENTS

The authors appreciate the insights from previous studies that informed the parameter values and modelling framework used in this work.

REFERENCES

Ali, M., Nelson, A. R., Lopez, A. L., & Sack, D. A. (2015). Updated global burden of cholera in endemic countries. *PLOS Neglected Tropical Diseases, 9*(6), Article e0003832. [Crossref]

Alshomrani, N. A. M., Alharbi, W. G., Alanazi, I. M. A., Alyasi, L. S. M., Alrefaei, G. N. M., Al'amri, S. A., & Alanzi, A. H. Q. (2024). Homotopy perturbation method for solving a nonlinear system for an epidemic. *Advances in Differential Equations and Control Processes, 31*(3), 347–355. [Crossref]

Alsubaie, A. A., Aljoufi, M. D., Alotaibi, A. G. S., Alfaydi, A. S. S., Alyoubi, R. M., Aljuhani, B. A. M., Alsahli, E. F. S., & Alanazi, B. S. (2024). Adomian's method for solving a nonlinear epidemic model. *Advances in Differential Equations and Control Processes, 31*(1), 95–107. [Crossref]

Azman, A. S., Rudolph, K. E., Cummings, D. A. T., & Lessler, J. (2013). The incubation period of cholera: A systematic review. *Journal of Infection, 66*(5), 432–438. [Crossref]

Bolaji, L. K., Sagir, A. M., & Balogun, F. (2024). Mathematical transmission dynamics and intervention strategies for monkeypox: A model-based approach including human-rodent interactions. *UMYU Scientifica, 3*(4), 288–299. [Crossref]

CDC. (2024, May 16). About typhoid fever and paratyphoid fever. *Typhoid Fever and Paratyphoid Fever*. [Crossref]

Guglielmi, N., Iacomini, E., & Viguerie, A. (2022). Delay differential equations for the spatially resolved simulation of epidemics with specific application to COVID-19. *Mathematical Methods in the Applied Sciences, 45*(8), 4752–4771. [Crossref]

Kailan Suhuyini, A., & Seidu, B. (2023). A mathematical model on the transmission dynamics of typhoid fever with treatment and booster vaccination. *Frontiers in Applied Mathematics and Statistics, 9*. [Crossref]

Kolawole, M. K., & Adebayo, S. R. (2025). Mathematical modeling of cholera transmission capturing vaccine effect and age structure using homotopy perturbation method. *Euler: Jurnal Ilmiah Matematika, Sains dan Teknologi, 13*(2), 157–168. [Crossref]

Kumar, P. V., Balaganesan, P., & Renuka, J. (2024). Mathematical analysis of malaria and cholera disease by homotopy perturbation method. *Journal of Communicable Diseases, 56*(1), 57–69. [Crossref]

Popoola, M. K., K., A. O., Odeyemi, K. A., & Bashiru, K. A. (2023). An approximate solution of fractional order epidemic model of typhoid using the homotopy perturbation method. *Uniosun Journal of Engineering and Environmental Sciences, 5*(1).

Marks, F., Von Kalckreuth, V., Aaby, P., Adu-Sarkodie, Y., El Tayeb, M. A., Ali, M., Aseffa, A., Baker, S., Biggs, H. M., Bjerregaard-Andersen, M., Breiman, R. F., Campbell, J. I., Cosmas, L., Crump, J. A., Espinoza, L. M. C., Deerin, J. F., Dekker, D. M., Fields, B. S., Gasmelseed, N., … Wierzba, T. F. (2017). Incidence of invasive salmonella disease in sub-Saharan Africa: A multicentre population-based surveillance study. *The Lancet Global Health, 5*(3), e310–e323. [Crossref]

Matsebula, L., & Nyabadza, F. (2022). Mathematical analysis of cholera typhoid co-infection transmission dynamics. *Frontiers in Applied Mathematics and Statistics, 8*, Article 892098. [Crossref]

Nigeria Centre for Disease Control and Prevention. (n.d.). Retrieved March 12, 2026, from [Link]

Ogunniyi, T. J., Muoneke, A. P., Nimo, F., Yisa, S. S., & Olorunfemi, O. A. (2025). Cholera in Nigeria: A five-decade review of outbreak dynamics and health system responses. *Journal of Health, Population and Nutrition, 44*(1), Article 329. [Crossref]

Panja, P. (2019). Optimal control analysis of a cholera epidemic model. *Biophysical Reviews and Letters, 14*(1), 27–48. [Crossref]

Rabiu, M., Abdulkadir, B., Aliyu, I. A., & Kumurya, A. S. (2022). Systematic review on the antibacterial resistance of *Vibrio cholerae*. *UMYU Scientifica, 1*(1), 60–66. [Crossref]

Rafiullah, M., Asif, M., Jabeen, D., & Ibrahim, M. A. (2024). Study of the six-compartment nonlinear

COVID-19 model with the homotopy perturbation method. *Axioms, 13*(5), Article 311. [Crossref]

Raza, A., Ahmed, N., Rafiq, M., Akgül, A., Cordero, A., & Torregrosa, J. R. (2024). Mathematical modeling of Ebola using delay differential equations. *Modeling Earth Systems and Environment, 10*(5), 6309–6322. [Crossref]

Stanaway, J. D., Reiner, R. C., Blacker, B. F., Goldberg, E. M., Khalil, I. A., Troeger, C. E., Andrews, J. R., Bhutta, Z. A., Crump, J. A., Im, J., Marks, F., Mintz, E., Park, S. E., Zaidi, A. K. M., Abebe, Z., Abejie, A. N., Adedeji, I. A., Ali, B. A., Amare, A. T., … Hay, S. I. (2019). The global burden of typhoid and paratyphoid fevers: A systematic analysis for the Global Burden of Disease Study 2017. *The Lancet Infectious Diseases, 19*(4), 369–381. [Crossref]

Tien, J. H., & Earn, D. J. D. (2010). Multiple transmission pathways and disease dynamics in a waterborne pathogen model. *Bulletin of Mathematical Biology, 72*(6), 1506–1533. [Crossref]

van den Driessche, P., & Watmough, J. (2002). Reproduction numbers and sub-threshold endemic equilibria for compartmental models of disease transmission. *Mathematical Biosciences, 180*(1), 29–48. [Crossref]

Wang, J., & Liao, S. (2012). A generalized cholera model and epidemic-endemic analysis. *Journal of Biological Dynamics, 6*(2), 568–589. [Crossref]

WHO Immunization Data portal-Detail Page. (n.d.). *Immunization Data*. Retrieved March 12, 2026, from [Link]

Yang, C. (2020). *Mathematical modeling, analysis, and simulation of cholera dynamics* [Master's thesis, institution name]. [Link]